Sensitivity of Metal Nanoparticle Surface Plasmon Resonance to the Dielectric Environment

Molly M. Miller and Anne A. Lazarides*

Department of Mechanical Engineering and Materials Science, Duke University, Box 90300, Durham, North Carolina 27708-0300

Received: July 29, 2005; In Final Form: August 25, 2005

Electrodynamic simulations of gold nanoparticle spectra were used to investigate the sensitivity of localized surface plasmon band position to the refractive index, n, of the medium for nanoparticles of various shapes and nanoshells of various structures. Among single-component nanoparticles less than 130 nm in size, sensitivities of dipole resonance positions to bulk refractive index are found to depend only upon the wavelength of the resonance and the dielectric properties of the metal and the medium. Among particle plasmons that peak in the frequency range where the real part of the metal dielectric function varies linearly with wavelength and the imaginary part is small and slowly varying, the sensitivity of the peak wavelength, λ^*, to refractive index, n, is found to be a linearly increasing function of λ^*, regardless of the structural features of the particle that determine λ^*. Quasistatic theory is used to derive an analytical expression for the refractive index sensitivity of small particle plasmon peaks. Through this analysis, the dependence of sensitivity on band position is found to be determined by the wavelength dependence of the real part, ϵ', of the particle dielectric function, and the sensitivity results are found to extend to all particles with resonance conditions of the form, $\epsilon'^* = -2\chi n^2$, where χ is a function of geometric parameters and other constants. The sensitivity results observed using accurate computational methods for dipolar plasmon bands of gold nanodisks, nanorods, and hollow nanoshells extend, therefore, to particles of other shapes (such as hexagonal and chopped tetrahedral), composed of other metals, and to higher-order modes. The bulk refractive index sensitivity yielded by the theory serves as an upper bound to sensitivities of nanoparticles on dielectric substrates and sensitivities of nanoparticles to local refractive index changes, such as those associated with biomolecule sensing.

I. Introduction

Noble metal nanoparticles and nanoshells support surface plasmons at optical frequencies, known as localized surface plasmons (LSPs).[1,2] The frequencies and intensities of LSP resonances are known to be sensitive to the dielectric properties of the medium,[3−14] and in particular, to the refractive index (RI) of matter close to the particle surface.[3,6,7,15−19] The local nature of nanoparticle surface plasmon RI sensitivity has led to the development of nanoparticles as biosensors.[16,20−22] Nanoparticle biosensors consist of particles functionalized with target molecule receptors whose LSP resonances are shifted, damped, or enhanced in the presence of target molecules. These changes in the nanoparticle optical properties signal the presence of target molecules. The magnitude of nanoparticle response to a local RI change is a function of the thickness of the layer displaying RI contrast and of the sensitivity of the resonance to changes in the RI of the bulk environment. Here, we focus upon this latter dependence, which provides an upper bound to the RI sensitivity of nanobiosensors composed of uncoupled nanoparticles.

Measurements and simulations of nanoparticle LSP resonance sensitivity to both bulk and local refractive index, n, are ongoing in many groups.[1−23] In general, plasmon resonances have been found to shift to the red as n is increased. More specifically, for a variety of nanoparticles, the peak wavelength, λ^*, has been found to increase linearly with n.[3−5,7−10,23] However, the peak wavelength sensitivities of plasmons supported by nanoparticles of various sizes, shapes, and compositions differ greatly.[4,8,10] Considering only the RI sensitivities of the lowest-energy, dipolar resonances, values of $d\lambda^*/dn$ ranging from tens to hundreds of nanometers have been observed for various nanoparticles, such as nanotriangles,[4,7,17] nanoplates,[5] nanorods,[23] nanospheres,[9,16] and nanoshells,[9,10] with high-aspect-ratio particles and thin nanoshells having the higher sensitivities. While for particles of a given structural class (i.e. rods, nanoshells), the dependence of $d\lambda^*/dn$ upon structural parameters is fairly well documented, there are no existing explanations for the relationships between the refractive index sensitivities of resonance location across particle classes. Here, using accurate electrodynamic calculations of nanoparticle spectra, we investigate the sensitivity of dipolar LSP resonance peak location to changes in bulk refractive index for several particle classes, with the goal of discovering principles that control sensitivity and developing tools that can be used to predict it.

The refractive index sensitivities investigated here are the sensitivities of plasmon band location, as manifest in extinction spectra. The extinction cross section, C_{ext}, of a particle is proportional to the imaginary part of the particle polarizability, α,

$$C_{ext} = 4\pi k \mathrm{Im}\{\alpha\} \quad (1)$$

where k is the magnitude $2\pi n/\lambda$ of the wavevector in the medium. For all particles, the resonance whose sensitivity was investigated was the lowest-energy dipolar mode, which for nanocylinders is a longitudinal mode and for nanodisks is an in-plane mode. Sensitivities of the resonance peak location to refractive index were determined by calculating extinction

* Corresponding author. E-mail: aal@duke.edu.

10.1021/jp054227y CCC: $30.25
Published on Web 10/21/2005

spectra of particles in two media, water ($n = 1.33$), and a higher-index ($n = 1.41$) medium representative of biomatter. The particles considered are small relative to the wavelength of light, i.e., have size parameters, ka (a, the radius of an equivalent volume sphere), at resonance in water less than 1, and in most cases, substantially less than 1. While most of the particles are large enough to require electrodynamic theory to accurately predict their resonant behavior, and all spectral simulations and sensitivity calculations were performed using accurate electrodynamic methods, quasistatic analysis was used to interpret the results. Within each particle class, sensitivities were calculated for particles of various aspect ratios.

Section II outlines the spectral simulation methods. Refractive index sensitivity results for cylinders, disks, solid nanoshells, and hollow nanoshells are presented in Section III, along with an approximate analytical theory developed to aide interpretation of the results. Section IV is a discussion focused on application of the results for prediction of nanoparticle RI sensitivities. Conclusions are summarized in Section V.

II. Electrodynamic Methods

Spectral simulations were performed using electrodynamic methods appropriate to the particle shape. The spectra of spherical nanoshells were calculated using Mie theory, which is exact for particles with spherical symmetry. The spectra of nanocylinders and nanodisks were calculated using the discrete dipole approximation[24,25] (DDA) on a cubic grid with a lattice constant equal to 1 nm. The DDA with a 1 nm lattice constant has been shown to yield accurate results for metal nanospheres in water.[26] All spectra were calculated using optical "constants" from Palik.[27] The sensitivity of the peak wavelength of the plasmon band to bulk refractive index is determined by taking the difference between peak wavelengths of the plasmon band of particles in media of refractive index, n, equal to 1.41, and peak wavelengths for particles in media of refractive index, n, equal to 1.33.

A. Mie Theory. Mie theory provides an exact description of the interaction of electromagnetic radiation with spherically symmetric particles in a dielectric medium.[2] The theory is exact and accurate insofar as the dielectric functions used to describe the material properly describe the polarization properties of the particle. For metal particles that are small relative to the electron mean free path, the wavelength-dependent dielectric functions used to calculate the polarizabilities are corrected from their bulk values to account for additional damping of the plasmon excitations at a nanoparticle surface.[28,29] The Mie solution consists of scattering coefficients, a_i or b_i, for each mode (electric dipole, magnetic dipole, electric quadrupole, etc) from which fields, cross sections, and efficiencies can be calculated as a function of wavelength. As with solid nanospheres, the extinction cross section of a nanoshell in light of a given vacuum wavelength, λ, has the form

$$C_{\text{ext}}(\lambda) = \frac{2\pi}{k^2}\sum_{i=1}^{\infty}(2i+1)\text{Re}\{a_i + b_i\} \tag{2}$$

where k is the magnitude of the wavevector in the medium, $2\pi n/\lambda$. Whereas, for solid nanospheres, the coefficients, a_i and b_i , are determined by the particle radius; for nanoshells, the coefficients are also a function of the inner radius, r_i, of the shell.[30] Single particle extinction cross sections are normalized by the geometric cross section, $C_{\text{geom}} = \pi r^2$, yielding efficiencies, $Q_{\text{ext}} = C_{\text{ext}}/C_{\text{geom}}$.

B. Discrete Dipole Approximation. Accurate electrodynamic responses to plane wave excitation can be calculated for particles of arbitrary shape using any of a number of time-independent[31−33] or time-dependent[34,35] methods. Here, we use a computationally efficient, time-independent method, the discrete dipole approximation (DDA), as developed and implemented by Draine, Goodman, and Flatau.[32,35,36] A given particle is represented as a cubic array of point dipoles, each with a polarizability determined by the particle dielectric function and the lattice parameter of the computational grid. Lattice dipole polarizabilities, α_i, are corrected from the electrostatic values for a sphere with volume equivalent to that of a lattice element, so as to yield wave propagation through the computational lattice that is consistent with the dispersion relation of bulk metal. The response of a particle to a monochromatic, electromagnetic wave is determined through a self-consistent solution of the coupled equations that determine the polarizations of the lattice elements. Each lattice element polarization vector, $\mathbf{P}_i$,

$$\mathbf{P}_i = \alpha_i \mathbf{E}_{\text{loc}}(\mathbf{r}_i) \tag{3}$$

is proportional to the local electric field, $\mathbf{E}_{\text{loc}}$. The local field, $\alpha_i^{-1}\mathbf{P}_i$, at a given lattice position, $\mathbf{r}_i$, is a sum of the incident field and the fields of all the other polarizations,

$$\alpha_i^{-1}\mathbf{P}_i = \mathbf{E}_o \exp(i\mathbf{k}\cdot\mathbf{r}) - \sum_{j\neq i}\mathbf{A}_{ij}\cdot\mathbf{P}_j \tag{4}$$

where $\mathbf{k}$ is the wave vector of the incident light and $\mathbf{A}_{ij}$ is a 3×3 tensor that determines the contribution

$$\mathbf{A}_{ij}\cdot\mathbf{P}_j = \frac{\exp(ik\mathbf{r})}{\mathbf{r}_{ij}^{\,3}}\left[k^2\mathbf{r}_{ij}\times(\mathbf{r}_{ij}\times\mathbf{P}_j) + \frac{(1-ik\mathbf{r}_{ij})}{\mathbf{r}_{ij}^{\,2}}\{\mathbf{r}_{ij}^{\,2}\mathbf{P}_j - 3\mathbf{r}_{ij}(\mathbf{r}_{ij}\cdot\mathbf{P}_j)\}\right] \tag{5}$$

to the local field at dipole i due to the polarization, $\mathbf{P}_j$, at location j. If a particle is represented by N dipole elements, the N polarization vectors are determined by simultaneous solution of $3N$ complex, linear equations. For particles in a dielectric medium, the magnitude of the wave vector, k, is $2\pi n/\lambda$, and the electrodynamic response is determined by the particle geometry, and the dielectric contrast between the particle and the medium. Extinction cross sections are calculated from the resulting polarizations as

$$C_{\text{ext}}(\lambda) = \frac{4\pi k}{|\mathbf{E}_0|^2}\sum_{j=1}^{N}\text{Im}\{\mathbf{E}_{\text{inc},j}^{*}\cdot\mathbf{P}_j\}. \tag{6}$$

In this work, extinction cross sections are expressed as efficiencies, $Q_{\text{ext}} = C_{\text{ext}}/C_{\text{geom}}$, i.e., optical cross sections normalized by a geometric cross section, C_{geom}. Solid particle spectra are calculated for particles oriented with a long axis parallel to the electric field of the incident light such that the longitudinal dipole mode is excited. The geometric cross sections used for normalization are, nonetheless, the cross sections of equal volume spheres.

III. Results

A. Solid Nanoparticles. Rodlike nanoparticles support longitudinal, dipolar LSP resonances with natural frequencies that are strongly dependent upon aspect ratio. Rods with higher aspect ratios have been observed to support resonances at lower frequencies that are excited by light of longer wavelength.[37−40] Calculated spectra for three gold nanocylinders, 20 nm in

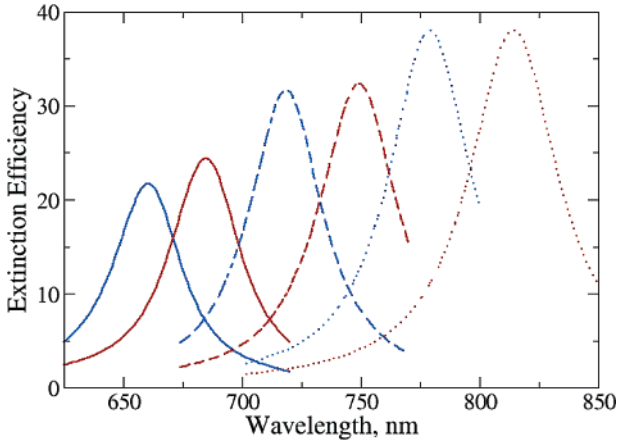

Figure 1. Extinction spectra, calculated using DDA, of gold nanocylinders in two media. 40 nm × 20 nm cylinders (solid line), 50 nm × 20 nm cylinders (dashed line), and 60 nm × 20 nm cylinders (dotted line) in $n = 1.33$ medium (blue) and $n = 1.41$ medium (red).

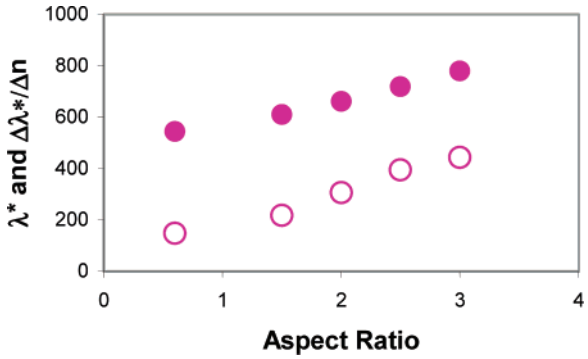

Figure 2. Peak plasmon wavelength (solid circles) and sensitivity of peak wavelength to the refractive index of the medium (open circles) for 20-nm-diameter gold cylinders, including the ones for which spectra are plotted in Figure 1, a 30 nm × 20 nm cylinder and a low-aspect-ratio "cylinder", 20 nm in diameter and 12 nm high.

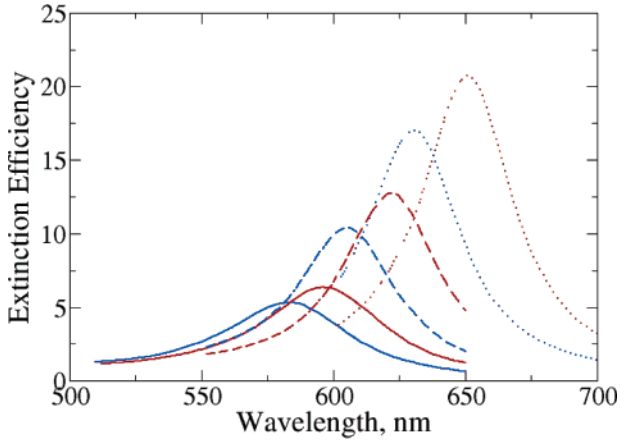

Figure 3. Extinction spectra of gold nanodisks in two media. Spectra are shown for 30 nm × 12 nm disks (solid lines), 40 nm × 12 nm disks (dashed lines), and 50 nm × 12 nm disks (dotted lines) in water ($n = 1.33$, blue) and a biomolecule medium ($n = 1.41$, red).

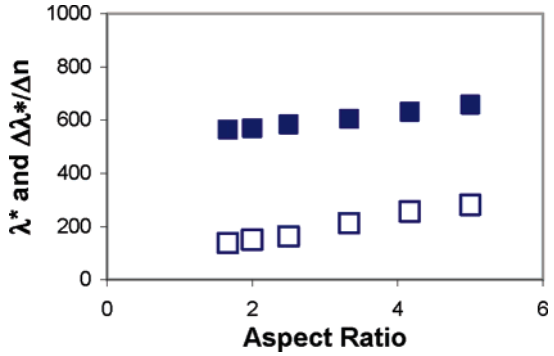

Figure 4. Structural dependence of the peak particle plasmon wavelength (solid squares) and of the sensitivity of the peak wavelength to bulk refractive index (open squares) for the 12-nm-thick disks for which spectra were plotted in Figure 3 as well as for 20 nm × 10 nm, 20 nm × 12 nm, and 60 nm × 12 nm disks.

diameter and with aspect ratios (length to diameter) of 2, 2.5, and 3, are illustrated in Figure 1. Resonant wavelengths, λ^*, for the cylinders in water (blue lines) vary from 660 to 780 nm. The resonant wavelengths for these cylinders and two lower-aspect-ratio cylinders are plotted (solid circles) as a function of aspect ratio in Figure 2. The lowest-aspect-ratio cylinder has a height smaller than the diameter and is, therefore, disklike in shape but is illuminated along its longitudinal axis and, therefore, behaves like a cylinder and is included here. Sensitivities of the peak wavelengths to the refractive index of the medium were determined by calculating spectra of the particles in two media, with refractive indices, n, equal to 1.33 (corresponding to water) and 1.41 (corresponding to organic matter with a dielectric constant of 2), and approximating the derivative, $d\lambda^*/dn$, with the ratio of variations, $\Delta\lambda^*/\Delta n$. The effect of this small variation in the refractive index of the medium on the nanocylinder spectra is illustrated in Figure 1 and summarized (hollow circles) in Figure 2. Band shifts induced by the 0.08 variation in refractive index vary from 11 nm for a short "cylinder" with an aspect ratio of 0.6 to 35 nm for a cylinder with an aspect ratio of 3.0. The dependence on aspect ratio of both the resonant wavelength and the sensitivity of the resonant wavelength to bulk refractive index of the medium is linear for particles in this size range, i.e., with size parameters, ka, less than 0.18, where a is the radius of a sphere of equal volume. Note that the short "cylinder" (20 nm diameter, 12 nm height) is disklike in shape and is excited transverse to its longest dimension, but is included here because the monitored excitation is parallel to the axis of rotational symmetry, as are the longitudinal resonances of the true cylinders whose behavior is summarized here.

Another class of metal nanostructures whose plasmonic properties and LSP resonance sensitivities have been investigated are the nanoplates, such as nanotriangles[4,7,17] and nanodisks.[5] Here, we consider the refractive index sensitivities of the in-plane dipole resonance of gold nanodisks of various aspect ratios, where aspect ratio is defined as the ratio of diameter to height. Extinction spectra of disks in water were calculated for disks with aspect ratios varying from 1.67 to 10, and size parameters at resonance between 0.13 and 0.26. Extinction spectra for disks of aspect ratio 2.5, 3.3, and 4.2 are shown in Figure 3. Peak wavelengths for a larger group of disks in water are shown in Figure 4 as solid squares. As expected, the in-plane dipole resonance peaks at longer wavelengths for nanodisks of higher aspect ratio. Peak wavelength sensitivities to refractive index (open squares), derived from spectra calculated at refractive indices 1.33 and 1.41 (Figure 3), are also shown in Figure 4. For disks in this size range, both peak wavelength sensitivities and peak wavelengths increase approximately linearly with aspect ratio.

From these sensitivity studies, it is apparent that, for nanocylinders and nanodisks with size parameters less than 0.26, the sensitivity of the wavelength of the lowest energy, dipolar resonance to refractive index of the medium increases with aspect ratio and is strongly correlated with the peak wavelength of the resonance, which also increases with aspect ratio. The

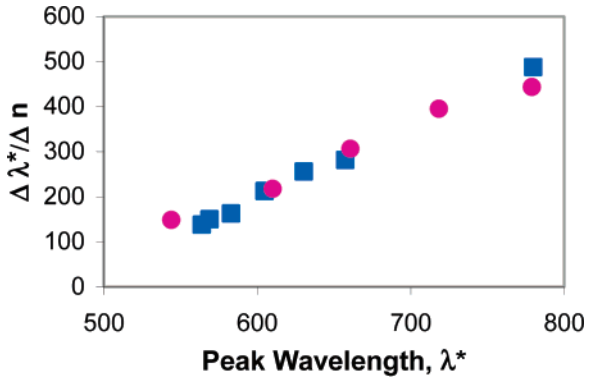

Figure 5. Sensitivity of LSP peak wavelength to bulk refractive index as a function of peak wavelength for gold nanodisks (squares) and cylinders (circles) of size parameter less than 0.26. Cylinders and disks are as in Figures 2 and 4 with the addition of a high-aspect-ratio, ultrathin 60 nm × 6 nm disk.

nature of the correlation is captured in Figure 5, where sensitivity is plotted as a function of peak wavelength for both classes of particles. For these nanostructures, whose low-energy dipolar resonances extend from 550 nm through the red end of the visible spectrum, the sensitivity of the resonant wavelength to bulk refractive index increases linearly with resonant wavelength and is independent of particle class.

B. Analytical Approximation to the Peak Wavelength Sensitivity. To explain the structural independence of the refractive index sensitivity of the LSP resonance band position and its linear dependence on band position, we have developed, using quasistatic theory, an approximate analytical expression for the sensitivity, $d\lambda^*/dn$, of the resonance wavelength to the refractive index of the medium. The refractive index sensitivity of the resonance is determined by the same two relations that determine the wavelength, λ^*, of the plasmon peak, namely the resonance condition, which, for a given particle structure, determines the real part, ϵ'^*, of the dielectric function at resonance given n, and the wavelength dependence of the dielectric function, which determines λ^* given ϵ'^*.

$$\frac{d\lambda^*}{dn} = \frac{\frac{d\epsilon'^*}{dn}}{\left(\frac{d\epsilon'(\lambda)}{d\lambda}\right)_{\lambda^*}} \tag{7}$$

According to this relation, the refractive index sensitivity of the peak wavelength is inversely proportional to the slope of the real part of the particle dielectric function and is otherwise determined by the refractive index dependence of the resonance condition. Noble metals have free electron-like dielectric functions that vary quadratically with wavelength. Using this Drude-like model for the dielectric function, others have investigated the dependence of the peak wavelength on refractive index for noble metal nanoparticles in dielectric media.[4,11,19] However, for each noble metal, in the part of the visible range to the red of the small particle limit to the LSP frequency, the real part of the dielectric function varies nearly linearly with wavelength and can be approximated using two parameters, ϵ_0 and m, as

$$\epsilon' \approx m\lambda + \epsilon_0 \tag{8}$$

where $m = d\epsilon'(\lambda)/d\lambda$ is the slope. For wavelengths between 500 and 800 nm, the real part of the gold dielectric function[27] can be fit with the linear form (eq 8) using 34 and −0.072 for ϵ_0 and m, respectively.[11] Because of the contribution of interband transitions to the dielectric function, the linear parametrization of ϵ' provides a more accurate representation of the slope of ϵ' in this range than does a quadratic Drude form parameterized to match ϵ'. Using the linear parametrization, eq 7 takes the form

$$\frac{d\lambda^*}{dn} = \frac{1}{m}\frac{d\epsilon'^*}{dn} \tag{9}$$

For solid particles much smaller than the wavelength of light, the polarizability is approximated by the quasistatic polarizability,

$$\alpha = \frac{3V}{4\pi}\frac{\epsilon - n^2}{n^2 + L(\epsilon - n^2)} \tag{10}$$

where ϵ ($= \epsilon' + i\epsilon''$) is the particle dielectric function, n is the refractive index of the solvent, L is the shape-dependent depolarization parameter, and V is the volume.[2] Resonance occurs at poles of the polarizability. At wavelengths where the imaginary part, ϵ'', of the metal dielectric function is small or slowly varying, the pole of the polarizability is found by setting the real part of the denominator of eq 10 to zero. The resulting resonance condition

$$\mathrm{Re}\{\epsilon^*\} = -n^2\left(\frac{1-L}{L}\right) \tag{11}$$

determines the value of the real part of the dielectric function at resonance. For the case of a sphere, the shape parameter, L, equals $^1/_3$, and eq 11 reduces to the familiar relationship $\mathrm{Re}\{\epsilon^*\} = -2n^2$, or $\epsilon'^* = -2n^2$ where $\epsilon'^* = \mathrm{Re}\{\epsilon^*\}$. For the general case, we define another shape-dependent parameter, χ,

$$\chi = \frac{1}{2}\left(\frac{1-L}{L}\right) \tag{12}$$

such that the resonance condition assumes a shape-parametrized form,

$$\epsilon'^* = -2\chi n^2 \tag{13}$$

χ is 1 for a sphere and greater than 1 for other particles, those with larger aspect ratios and smaller depolarization parameters. Higher-order modes satisfy resonance conditions of the form of eq 13, with other values of χ.

The resonance condition influences the sensitivity of the peak wavelength to the refractive index of the medium through its derivative with respect to n,

$$\frac{d\epsilon'^*}{dn} = -4\chi n \tag{14}$$

The relation can be rewritten as

$$\frac{d\epsilon'^*}{dn} = \frac{2}{n}\epsilon'^* \tag{15}$$

such that eq 7 becomes

$$\frac{d\lambda^*}{dn} = \frac{2\epsilon'^*}{n\left(\frac{d\epsilon'(\lambda)}{d\lambda}\right)_{\lambda^*}} \tag{16}$$

In the wavelength range where the real part of the nanoparticle dielectric function varies linearly with wavelength, the derivative in the denominator can be replaced by the constant slope, m, and eq 9 becomes

$$\frac{d\lambda^*}{dn} = \frac{2}{n}\left(\frac{\epsilon'^*}{m}\right) \tag{17}$$

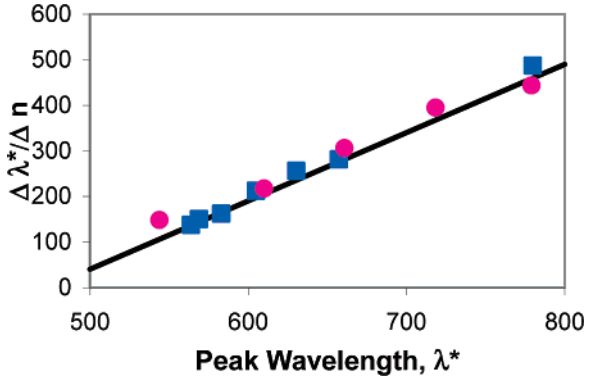

Figure 6. Sensitivity of peak wavelength to bulk refractive index for cylinders (circles), disks (squares), and the analytical approximation, $d\lambda^*/dn = 1.5\lambda^* - 710$ (solid line).

Replacing ϵ'^* by its linear parametrization, eq 8, yields an expression for the refractive index sensitivity of the plasmon peak wavelength,

$$\frac{d\lambda^*}{dn} = \frac{2}{n}\lambda^* + \frac{2}{n}\frac{\epsilon_0}{m} \tag{18}$$

that is linear in peak wavelength, λ^*. The slope, $2/n$, and intercept, $2\epsilon_0/nm$, that parametrize the linear form are determined exclusively by the refractive index of the medium, n, and the linear parametrization, ϵ_0 and m, of the real part of the dielectric function of the nanoparticle. A plot of this expression for the sensitivity as a function of wavelength for a gold nanoparticle ($\epsilon_0 = 43$, $m = -0.072$) in water ($n = 1.33$) is shown in Figure 6. Also plotted are the calculated results for gold nanocylinders and nanodisks, reproduced from Figure 5.

The close match between the accurately calculated sensitivities and the analytical estimates based on quasistatic theory suggest that the analytical expression (eq 18) for the refractive index sensitivity is valid under a broader range of conditions than those under which quasistatic theory is valid. Elsewhere, we report on an analysis of the validity of the sensitivity expression given by eq 16 for larger particles.[41] Thus, the subsuming of the geometry dependence of the sensitivity in the geometry dependence of the band location may be a broadly applicable result. From the derivation of the analytical results, it is clear that, apart from material properties, the refractive index sensitivity of the LSP sensitivity is determined by the structure of the resonance condition and its derivative with respect to refractive index. In what follows, we will examine the LSP sensitivities of other particles and the resonance conditions that control them.

C. Nanoshells. Having established that, among solid, single-component nanoparticles much smaller than the wavelength of light at resonance, the refractive index sensitivities of resonances are determined by the position of the plasmon band, and otherwise independent of particle shape, we became interested in understanding the extent of applicability of the result. In particular, we sought to determine whether the shape independence of the refractive index sensitivities of solid particles extends to nanoshells. Spherical nanoshells, like the solid nanoparticles considered above, have dipolar resonances that are tunable through the visible and near-IR spectrum[42-44] and high sensitivities to local refractive index that are desirable in refractive index-based biomolecule sensing.[10,20,42,43,45] Spherical gold nanoshells on gold sulfide cores have been shown to have higher peak wavelength sensitivity to solvent refractive index changes than solid nanoparticles of the same size.[13] While spherical nanoshells with solid dielectric cores have more tunable parameters (two radii and a core dielectric constant) than do the other nanoparticles considered here and, thus, may display a richer range of sensitivity behaviors, hollow nanoshells have the same number of tunable parameters as solid disks and cylinders. Here, we consider both nanoshells on solid dielectric cores and hollow nanoshells.

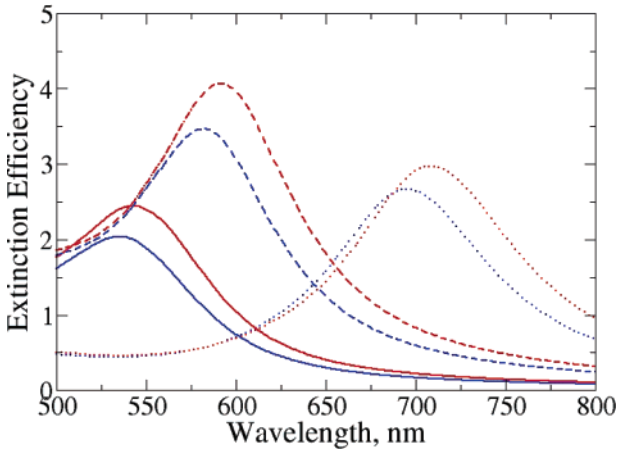

Figure 7. Extinction spectra of gold nanoshells on gold sulfide cores in two media calculated using Mie theory. Nanoshells: 5/15 nm (solid lines), 15/15 nm (dashed lines), and 15/5 nm (dotted lines) in media of refractive index $n = 1.33$ (blue) and $n = 1.41$ (red).

The refractive index sensitivities of gold nanoshell resonances were investigated using Mie theory.[2] As with the solid particle sensitivity study, the sensitivities of the peak wavelength to the refractive index of the medium were determined by comparing peak wavelengths of spectra calculated for particles in media of refractive index 1.33 and 1.41. Initially, we examined the refractive index sensitivities of nanoshells with solid cores of refractive index, $n_{in} = 2.332$, representative of nanoshells with gold sulfide cores. Spectra and sensitivities were calculated for nanoshells with diameters between 10 and 40 nm and aspect ratios between 0.25 and 0.83, where aspect ratio is defined as the ratio of core radius to shell radius. Spectra in both media for three of the particles are shown in Figure 7. Particle geometries are specified by r_1/t, where r_1 is the radius in nm of the core (inner radius of the shell) and t is the thickness in nm of the shell. As has been previously documented,[43,46] particles with larger aspect ratios, $r_1/(r_1 + t)$, i.e., thinner shells, have plasmon bands located at longer wavelengths. The red-shifts associated with increments of 0.08 in the refractive index increase from 8 nm for the low-aspect-ratio (thick-shelled) nanoshells to 17 nm for the high-aspect-ratio (thin-shelled) nanoshells. Resonant wavelengths of the nanoshells in water as a function of aspect ratio are summarized in Figure 8 (orange triangles). Among particles with aspect ratios below two-thirds, the resonant wavelength increases approximately linearly with aspect ratio; among particles with higher aspect ratios, the resonant wavelength increases more rapidly.

Sensitivities of the resonant wavelength to refractive index are also summarized in Figure 8 (hollow triangles) and display weak and strong dependence upon aspect ratio for the same ranges of aspect ratio as do the band locations. While both band location and sensitivity to refractive index depend nonlinearly upon aspect ratio, band location and sensitivity appear to be strongly correlated with each other, as was observed for solid, single-component nanoparticles.

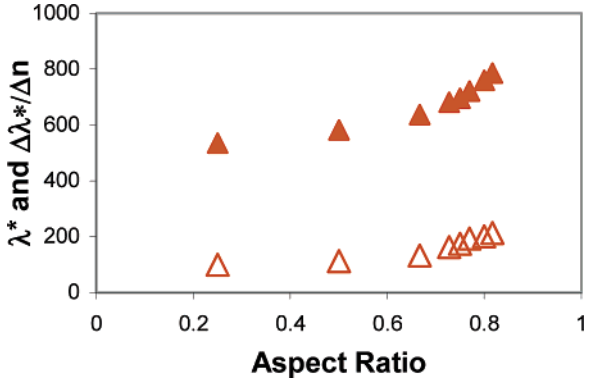

Figure 8. Dependence on aspect ratio of Au/Au_2S nanoshell plasmon peaks (solid triangles) and the sensitivity of the peaks to refractive index of the external medium (open triangles). The Au_2S core has a refractive index of 2.332. Nanoshells with plasmon peaks and peak sensitivities to refractive index that depend weakly upon aspect ratio have core radii, r_1, and shell thicknesses, t, of 5/15, 15/15, and 15/7.5 nm. Higher-aspect-ratio nanoshells with peaks and sensitivities that vary rapidly with aspect ratio have r_1/t of 20/7.5, 15/5, 20/6, 20/5, and 20/4.5 nm.

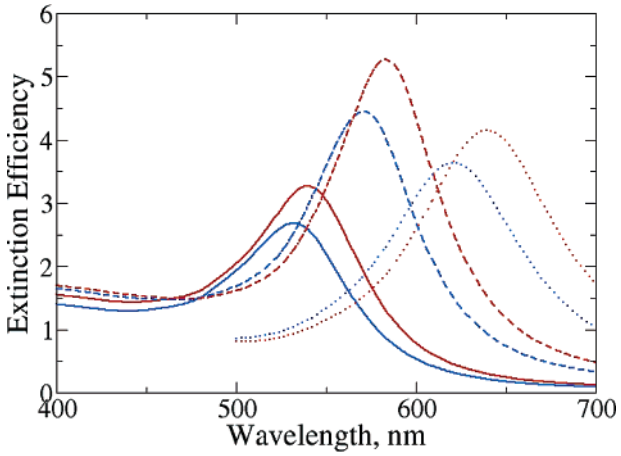

Figure 9. Extinction spectra of hollow gold nanoshells in two media. Nanoshell inner radii/shell thickness: 5/15 nm (solid lines), 15/15 nm (dashed lines), and 15/5 nm (dotted lines); refractive indices of the media inside and outside the shells are $n = 1.33$ (blue) and $n = 1.41$ (red).

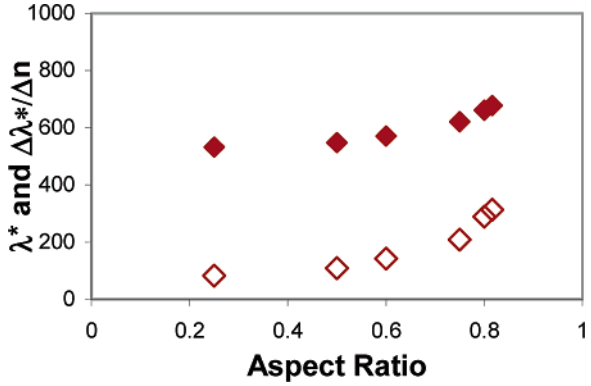

Figure 10. Dependence on aspect ratio of hollow gold nanoshell plasmon peaks (solid diamonds) and sensitivities of peaks to the refractive index of the medium (open diamonds). The refractive index of the medium (internal and external) is varied from 1.33 to 1.41. Nanoshells (r_1/t: 5/15, 10/10, and 15/15 nm) with aspect ratios less than 0.6 have resonant wavelengths and refractive index sensitivities that vary slowly with aspect ratio when compared with nanoshells (15/5, 20/5, and 20/4.5 nm) with aspect ratios greater than 0.7.

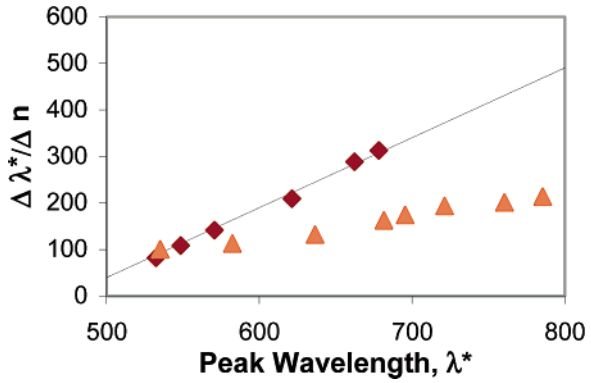

Figure 11. Sensitivity of peak wavelength to bulk refractive index for hollow gold nanoshells (diamonds) and solid nanoshells on gold sulfide ($n = 2.332$) cores (triangles). Solid nanoshell sensitivities are reproduced from Figure 8 and hollow nanoshell sensitivities are reproduced from Figure 10. The line that passes through the hollow nanoshell sensitivities is the peak wavelength-dependent sensitivity derived in Section IIIB for solid nanoparticles.

Refractive index sensitivities were calculated for hollow nanoshells as well. Extinction spectra for hollow nanoshells with the same shell geometries as the solid core nanoshells, for which spectra are given in Figure 7, are plotted in Figure 9. For the refractive index increment of 0.08 refractive index units from the index of water, red-shifts increase from 7 nm for the low-aspect-ratio (thick-shelled) nanoshells to 15 for the high-aspect-ratio (thin-shelled) nanoshells. Peak wavelengths and sensitivities of the wavelength to refractive index of the medium for these and other higher-aspect-ratio nanoshells are summarized in Figure 10. As with the solid core nanoshells, both the peak wavelength (solid diamonds) and the peak wavelength sensitivity (open diamonds) increase nonlinearly with aspect ratio, but appear to be strongly correlated with each other.

The positive correlation between peak wavelength, λ^*, and peak wavelength refractive index sensitivity, $d\lambda^*/dn$, apparent by comparison of the plots of the two quantities as a function of aspect ratio in Figure 8 and Figure 10 for solid and hollow gold nanoshells, respectively, is analogous to that identified in Section A for solid gold nanocylinders and nanodisks. Plots of refractive index sensitivity as a function of peak wavelength (Figure 11) quantify the correlation. Both solid (triangles) and hollow (diamonds) nanoshells have plasmon resonances with refractive index sensitivities that depend linearly upon resonance wavelength. Superposition of the sensitivity function (eq 18, originally shown in Figure 6) derived in Section B for solid metal nanoparticles indicates that the sensitivities of hollow shell plasmons to the refractive index of the medium are the same as those of solid metal nanoparticles with the same plasmon band locations, while those of nanoshells on solid cores of high dielectric constant, such as gold sulfide ($n = 2.332$), are smaller. The nanoshells for which sensitivities are illustrated have size parameters less than 0.44 (hollow nanoshells) and 0.36 (solid nanoshells).

Additional electrodynamic sensitivity calculations were performed for larger particles to determine whether particles that experience more phase retardation than the sub-60 nm shells considered above have refractive index sensitivities consistent with those of their smaller counterparts. Size parameters for hollow nanoshells were extended to 0.77, while those of solid nanoshells were extended to 0.69. Results of the calculations are illustrated in Figure 12 along with the small particle results. Larger hollow nanoshells (large diamonds) have refractive index sensitivities consistent with the analytical theory (eq 18) for solid, single-component nanoparticles, while larger solid

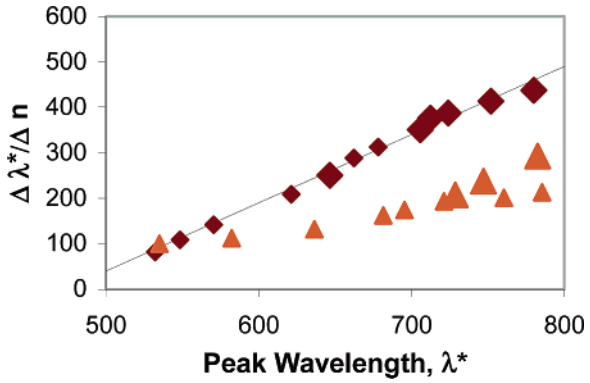

Figure 12. Sensitivity of peak wavelength to bulk refractive index for hollow gold nanoshells (diamonds) including larger particles (larger diamonds) of sizes 25/7.5, 50/15, 35/7.5, 25/4.5, 35/6, and 25/3.5 nm and gold nanoshells on Au_2S ($n = 2.332$) cores (triangles) including larger sizes (larger triangles), 25/7.5, 35/10.5, and 50/15 nm. The line that passes through the hollow nanoshell sensitivities is the peak wavelength-dependent sensitivity derived in Section IIIB for solid nanoparticles.

nanoshells (large triangles) have sensitivities that grow nonlinearly with band location, deviating initially from the linear line followed by smaller solid nanoshells at size parameters of 0.37. Hollow nanoshells, including nanoshells significant in size relative to the wavelength of resonant light, but not solid nanoshells, thus appear to have refractive index sensitivities that, like those of solid, single-component nanoparticles, are consistent with the analytical theory of Section B, that yields particle shape-independent sensitivities which, for gold nanoparticles with resonances in the visible (and slightly beyond), depend linearly upon resonance wavelength, with slope and intercept determined by the dielectric properties of the particle and medium.

D. Analytical Approximation to the Peak Wavelength Sensitivity: Extension to Nanoshells. The consistency between the refractive index sensitivities of hollow nanoshells and the shape-independent quasistatic sensitivity theory derived for solid, single-component nanoparticles in Section B suggests that there is a hollow nanoshell theory that yields the same sensitivity expression as that derived for solid particles. While the refractive index sensitivity expression matched by the hollow nanoshells is the linear form (eq 18) appropriate for plasmon bands in the linear range of the dielectric function, the coincidence of calculated hollow nanoshell and solid nanoparticle sensitivities suggests that the more general sensitivity expression, eq 16, not restricted to linear ranges of the dielectric function, also is applicable to hollow nanoshells. Both sensitivity expressions are derived using a resonance derivative equation (eq 15) that is satisfied by resonance conditions of the form $\epsilon'^* = -2\chi n^2$ and, therefore, are valid for any nanoparticle with a polarizability of the form

$$\alpha \propto \frac{\epsilon - n^2}{\epsilon + 2\chi n^2} \tag{19}$$

where χ is a constant.

A closed form expression for the quasistatic dipolar polarizability of a nanoshell has been determined previously.[42,45] The nanoshell polarizability depends on the dielectric function of the metal, ϵ, the medium, n_{out}^2, and the core, n_{in}^2, and upon the geometry of the particle through the shell volume fraction, P

$$\alpha \propto \frac{\epsilon\epsilon_a - n_{out}^2\epsilon_b}{\epsilon\epsilon_a + 2n_{out}^2\epsilon_b}$$

where

$$\begin{aligned} \epsilon_a &= n_{in}^2(3 - 2P) + 2\epsilon P \\ \epsilon_b &= n_{in}^2 P + \epsilon(3 - P) \\ P &= 1 - (r_{in}/r)^3 \end{aligned} \tag{20}$$

Whereas the denominator of the solid particle polarizability (eq 10) is linear with respect to the dielectric function, ϵ, the denominator of the nanoshell polarizability has a quadratic dependence upon the dielectric function, ϵ, because of the ϵ-dependence of ϵ_a and ϵ_b. Poles of the polarizability are found by setting the real part of the denominator to zero.

$$\mathrm{Re}\{\epsilon\epsilon_a + 2n_{out}^2\epsilon_b\} = 0 \tag{21}$$

In the wavelength range where the imaginary part, ϵ'', of the dielectric function is small relative to the real part, ϵ', contributions to the resonance condition from ϵ'' can be neglected, and eq 21 becomes a quadratic constraint on ϵ',

$$2P\epsilon'^2 + b\epsilon' + c = 0 \tag{22}$$

with constant coefficients, $2P$, b, and c

$$\begin{aligned} b &= n_{in}^2(3 - 2P) + 2n_{out}^2(3 - P) \\ c &= 2n_{in}^2 n_{out}^2 P \end{aligned} \tag{23}$$

determined by the shell volume fraction, P, as well as the refractive index of the medium, n_{out}, and of the core, n_{in}. Equation 22 has two real solutions

$$\epsilon_\pm = \frac{1}{4P}\left[-b \pm \sqrt{b^2 - 8Pc}\right] \tag{24}$$

among which ϵ_- is the value, ϵ'^*, of the real part of the dielectric function at the lowest-energy dipolar resonance. For nanoshells formed around solid dielectric cores, n_{in} differs from the variable n_{out}, and the resonance condition has a complex dependence on the internal and external refractive indices,

$$\epsilon'^* = \frac{1}{4P}\left[-(n_{in}^2(3 - 2P) + 2n_{out}^2(3 - P)) - \sqrt{(n_{in}^2(3 - 2P) + 2n_{out}^2(3 - P))^2 - 16P^2 n_{out}^2 n_{in}^2}\right] \tag{25}$$

For hollow nanoshells with an internal refractive index, n_{in}, that matches the external one, n_{out}, the resonance condition takes the simpler form

$$\epsilon'^* = \frac{n^2}{4P}\left[-(9 - 4P) - 3\sqrt{9 - 8P}\right] \tag{26}$$

where $n = n_{in} = n_{out}$.

From eqs 25 and 26, it is apparent that hollow nanoshells with index-matched interiors and exteriors, but not solid nanoshells, have a resonance condition of the form $\epsilon'^* = -2\chi n^2$, specifically with $\chi = ((9 - 4P) + 3\sqrt{9-8P})/8P$, such that the structure-independent sensitivity results (eqs 17 and 18), derived above for solid particles, are applicable. The analytical result for sensitivity of a hollow nanoshell plasmon to bulk refractive

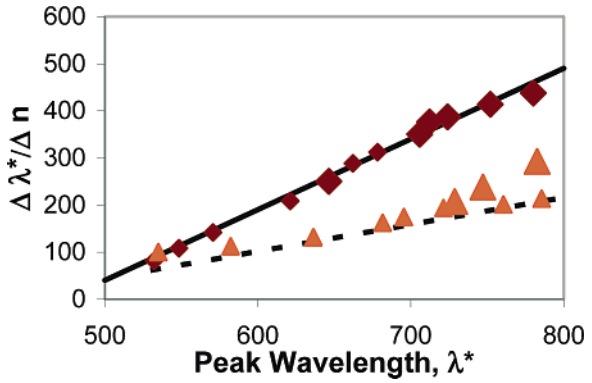

Figure 13. Sensitivity results for hollow nanoshells (diamonds) and solid nanoshells with $n = 2.332$ cores (triangles). Also shown are analytical results for hollow nanoshells (solid line), and nanoshells with $n = 2.332$ (gold sulfide) cores (dashed line).

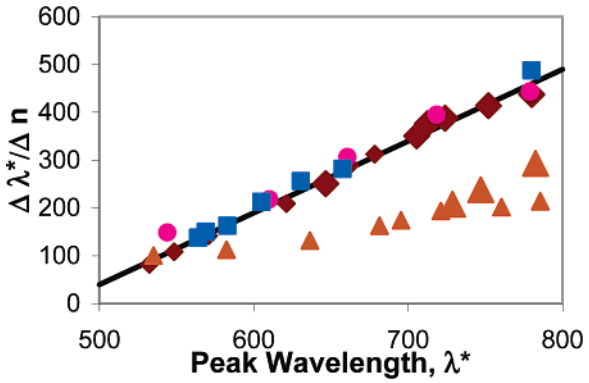

Figure 14. Linear relationship between peak plasmon wavelength and sensitivity of that wavelength to refractive index for nanocylinders (circles), nanodisks (squares), and hollow nanoshells (diamonds, larger diamonds showing larger hollow nanoshells). Solid nanoshells (triangles) with an $n = 2.332$ core are linear except for larger particles (larger triangles). The solid line shows the analytical fit of eq 18 using the parameters for gold.

index is the same as that for solid particles, as suggested by the accurate calculated sensitivities plotted in Figure 12 and again in Figure 13 (solid line). As with solid nanoparticles, the analytical sensitivity expression derived using quasistatic theory appears to be applicable to nanoshells much larger than those whose plasmonic behavior is accurately represented by quasistatic theory.

While nanoshells with solid dielectric cores have polarizabilities that do not fit the analytical structure required to invoke the single-component nanoparticle theory, the sensitivities of small nanoshells with solid cores do display a linear dependence upon band location that merits investigation. The quasistatic resonance condition (eq 25) can be used to determine explicitly the dependence of its refractive index derivative on shell fraction and inner and outer refractive indices. Substitution of the derivative of eq 25 with respect to the external refractive index into eq 9 yields the gold/gold sulfide nanoshell sensitivity (dashed line) illustrated in Figure 13. The analytical sensitivity appears to depend linearly upon band location in the visible range and is applicable to the smaller solid nanoshells, but not the larger ones.

The sensitivities of the gold/gold sulfide ($n = 2.332$) nanoshells fall well below the sensitivities of solid gold nanoparticles and hollow gold nanoshells. Both simulation and evaluation of eq 9 (results not shown), as well as prior investigations by others,[46,47] indicate that the sensitivity of a solid nanoshell to bulk refractive index decreases as the refractive index of the core material is increased. Thus, a nanoshell with a high refractive index core has a lower sensitivity to the external refractive index than a structurally identical particle with a lower index core. A gold nanoshell with a silica ($n = 1.439$) core exhibits sensitivities intermediate between those of a gold nanoshell with a gold sulfide ($n = 2.332$) core and a hollow gold nanoshell with the same resonance wavelength. In ongoing work, we are addressing the role of the solid cores and solid substrates on the refractive index sensitivities of nanoshells and nanoparticles, respectively.

By using both accurate computational methods and quasistatic theory, we have investigated the sensitivity of LSP peak wavelength to bulk refractive index for a diverse collection of gold nanoparticles and nanoshells. Sensitivities for all investigated particles are summarized in Figure 14. While nanoshells on high index dielectric cores (triangles) have lower sensitivities than single-component nanoparticles, nanocylinders, nanodisks and hollow nanoshells with peak wavelengths between 500 and 800 nm have sensitivities that depend linearly upon peak wavelength and are otherwise independent of nanoparticle shape.

IV. Discussion

As illustrated in Figure 14, for rods and disks up to 60 nm in size and hollow nanoshells up to 130 nm in diameter, the sensitivity of the plasmon peak wavelength of particles of nonnegligible size parameter to refractive index of the medium is determined by the location of the plasmon peak, regardless of nanoparticle structure or size. Any single-component nanoparticle with a polarizability of the form of eq 10 or a resonance condition of the form of eq 13 has a bulk refractive index sensitivity that can be estimated accurately from the extinction spectrum without collecting spectra of particles in multiple solvents. Within a range of wavelengths where the real part, ϵ', of the nanoparticle material's dielectric function varies linearly with wavelength and the imaginary part, ϵ'', is small and slowly varying, the refractive index sensitivity of small nanoparticles is also found to vary linearly with wavelength of the plasmon peak and can be calculated straightforwardly using eq 17 from the slope, m, and intercept, ϵ_0, of the linear fit, eq 8, to the real part of the nanoparticle dielectric function. For nanoparticles composed of gold with plasmon bands in the lower mid-500s to high 700s of nanometers, the wavelength dependence of the dielectric function is fit with parameters $\epsilon_0 = 34$ and $m = -0.072$ and the sensitivities equal $1.5\lambda^* - 710$. To evaluate the sensitivities of particles with resonances further into the infrared, other parameters determined by linearization of the dielectric function in the range of interest would be required. Alternatively, the region of interest of the dielectric function can be fit with a nonlinear function, which can be used in eq 16.

We demonstrate the sensitivity estimation method for a gold nanoparticle with a shape different from any of the shapes considered above. Spectral simulation of a prolate, 30 nm × 12 nm gold spheroid in water reveals a longitudinal dipole resonance at 640 nm. Equation 8 predicts a refractive index sensitivity of 252 nm per refractive index unit (riu) for a gold nanoparticle with a resonance in water at this wavelength. Note that *RI sensitivity could be estimated in this same simple way for any gold nanoparticle of moderate size from the location of its plasmon band, without knowledge of the structure of the particle*. Here, we evaluate the accuracy of the estimated sensitivity by performing another (fully electrodynamic) simula-

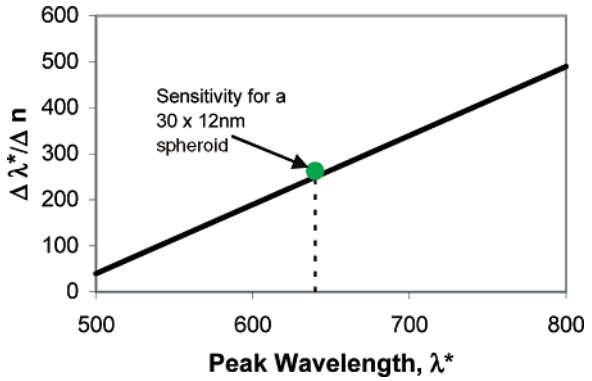

Figure 15. Comparison of estimated and calculated sensitivities of plasmon band location to refractive index. Estimates of sensitivities for particles with bands at various wavelengths are represented by a solid line. Accurately calculated sensitivity for a 30 nm × 12 nm solid Au spheroid is represented by a solid, green circle.

tion for the same particle in a medium of refractive index, n, equal to 1.41, and determining the RI sensitivity through evaluation of the finite difference ratio, $\Delta\lambda/\Delta n$. By comparison with this calculated sensitivity ($\Delta\lambda/\Delta n = 262.5$ nm per riu), the sensitivity, 252.3 nm per riu, estimated from the plasmon band location, is found to be in error by less than 4%. Figure 15 shows the good agreement between sensitivity determined by finite differences based on accurate spectral simulations and sensitivity estimated using the analytical sensitivity expression.

The LSPR sensitivity estimation method proposed here is useful as well for nanobiosensor design. While the environmental sensitivity of nanoparticle surface plasmon resonances is local, bulk sensitivities provide an upper bound to the sensitivity of a resonance to a finite molecular layer. The extent of the deviation of the biolayer sensitivity from the bulk sensitivity will be governed by the extent to which the biolayer fills the sensing volume of the particle for the given mode, a topic that we and others have discussed elsewhere.[16,17,22,48]

Having questioned the need for measuring bulk refractive index sensitivities when particles are in solution, it is important to point out the importance of experimental measurement of sensitivity when particles are supported on substrates. While the bulk refractive index sensitivities of nanoparticles in solution or in embedding media can be accurately determined without either measuring the sensitivity or knowing details of the particle structure, the reduction in sensitivity that accompanies assembly on a substrate is both shape and mode dependent. Similarly, the reduction in sensitivity associated with inducing dielectric variation in a molecular shell as opposed to in the extended bulk environment is also very sensitive to details in particle structure and lateral distribution of the molecular layer. Sensitivity measurements, therefore, are extremely useful for understanding the sensitivity of plasmon band location to local, or otherwise spatially constrained, variations in the dielectric properties of the environment.

V. Conclusions

By using accurate electrodynamic simulations of gold nanoparticles of significant size parameters, we have demonstrated that the sensitivity of a plasmon peak wavelength to a variation in refractive index of the environment is determined by the location of the peak wavelength and the dielectric properties of the material. Among single-component particles within the size ranges considered here, refractive index sensitivities are independent of particle shape, size, and composition, except through their control of band location. Using quasistatic theory, we have developed an analytical expression for the sensitivity of the band location to refractive index of the medium that applies to particles larger than those accurately modeled using quasistatic theory and can be generalized to modes not captured at all by static theory. Among localized surface plasmons of both solid nanoparticles and hollow nanoshells in the range of wavelengths where the dielectric function of the nanoparticle material varies linearly with wavelength, the refractive index sensitivities of plasmon band location vary linearly with band location. The bulk refractive index sensitivities considered here represent an upper bound to the refractive index sensitivities of particles on substrates or particles that experience refractive index changes that are local, as opposed to global. Reductions in sensitivities due to incomplete exchange of the medium can be expected to be highly shape, size, and mode dependent. Investigations of these phenomena are ongoing.

Acknowledgment. We acknowledge the support of the Centers for Disease Control through grant NCID R01 CI-00097 and the National Science Foundation for support in the form of an IGERT, DGE02-21632.

References and Notes

(1) Kreibig, U.; Vollmer, M. *Optical Properties of Metal Clusters*; Springer: Berlin, New York, 1995.
(2) Bohren, C. F.; Huffman, D. R. *Absorption and Scattering of Light by Small Particles*; John Wiley & Sons: New York, 1983.
(3) Haes, A. J.; Zou, S. L.; Schatz, G. C.; Van Duyne, R. P. *J. Phys. Chem. B* **2004**, *108*, 6961−6968.
(4) Jensen, T. R.; Duval, M. L.; Kelly, K. L.; Lazarides, A. A.; Schatz, G. C.; Van Duyne, R. P. *J. Phys. Chem. B* **1999**, *103*, 9846−9853.
(5) Hanarp, P.; Kall, M.; Sutherland, D. S. *J. Phys. Chem. B* **2003**, *107*, 5768−5772.
(6) Jensen, T. R.; Malinsky, M. D.; Haynes, C. L.; Van Duyne, R. P. *J. Phys. Chem. B* **2000**, *104*, 10549−10556.
(7) Malinsky, M. D.; Kelly, K. L.; Schatz, G. C.; Van Duyne, R. P. *J. Am. Chem. Soc.* **2001**, *123*, 1471−1482.
(8) Mock, J. J.; Smith, D. R.; Schultz, S. *Nano Lett.* **2003**, *3*, 485−491.
(9) Raschke, G.; Brogi, S.; Susha, A. S.; Rogach, A. L.; Klar, T. A.; Feldmann, J.; Fieres, B.; Petkov, N.; Bein, T.; Nichtl, A.; Kurzinger, K. *Nano Lett.* **2004**, *4*, 1853−1857.
(10) Tam, F.; Moran, C.; Halas, N. *J. Phys. Chem. B* **2004**, *108*, 17290−17294.
(11) Templeton, A. C.; Pietron, J. J.; Murray, R. W.; Mulvaney, P. *J. Phys. Chem. B* **2000**, *104*, 564−570.
(12) Sun, Y. G.; Xia, Y. N. *Analyst (Cambridge, U.K.)* **2003**, *128*, 686−691.
(13) Khlebtsov, N. G.; Trachuk, L. A.; Mel'nikov, A. G. *Opt. Spectrosk.* **2005**, *98*, 77−83.
(14) Trachuk, L. A.; Vrublevsky, S. A.; Khlebtsov, B. N.; Mel'nikov, A. G.; Khlebtsov, N. G. *SPIE, 2005*; Zimnyakov, D. A., Ed.; 2005; Vol. 5772, pp 1−10.
(15) Gole, A.; Murphy, C. J. *Chem. Mater.* **2005**, *17*, 1325−1330.
(16) Nath, N.; Chilkoti, A. *Anal. Chem.* **2002**, *74*, 504−509.
(17) Haes, A. J.; Zou, S. L.; Schatz, G. C.; Van Duyne, R. P. *J. Phys. Chem. B* **2004**, *108*, 109−116.
(18) Xu, H. X.; Kall, M. *Sens. Actuators, B* **2002**, *87*, 244−249.
(19) Khlebtsov, N. G. *J. Quant. Spectrosc. Radiat. Transf.* **2004**, *89*, 143−153.
(20) West, J. L.; Halas, N. J. *Annu. Rev. Biomed. Eng.* **2003**, 5285−5292.
(21) Lazarides, A. A.; Kelly, K. L.; Jensen, T. R.; Schatz, G. C. *J. Mol. Struct. THEOCHEM* **2000**, 52959−52963.
(22) Haes, A. J.; Hall, W. P.; Chang, L.; Klein, W. L.; Van Duyne, R. P. *Nano Lett.* **2004**, *4*, 1029−1034.
(23) Link, S.; Mohamed, M. B.; El-Sayed, M. A. *J. Phys. Chem. B* **1999**, *103*, 3073−3077.
(24) Draine, B. T. *Astrophys. J.* **1988**, *333*, 848−872.
(25) Yang, W. H.; Schatz, G. C.; Vanduyne, R. P. *J. Chem. Phys.* **1995**, *103*, 869−875.
(26) Hao, E.; Schatz, G. C. *J. Chem. Phys.* **2004**, *120*, 357−366.
(27) Palik, E. D. *Handbook of Optical Constants of Solids*; Academic: New York, 1985.
(28) Coronado, E. A.; Schatz, G. C. *J. Chem. Phys.* **2003**, *119*, 3926−3934.
(29) Kraus, W. A.; Schatz, G. C. *J. Chem. Phys.* **1983**, *79*, 6130−6139.

(30) Aden, A. L.; Kerker, M. *J. Appl. Phys.* **1951**, *22*, 1242−1246.
(31) Barber, P. W.; Hill, S. C. *Light Scattering by Particles: Computational Methods*; World Scientific: Singapore, 1990.
(32) Draine, B. T.; Goodman, J. *Astrophys. J.* **1993**, *405*, 685−697.
(33) Novotny, L.; Pohl, D. W.; Hecht, B. *Opt. Lett.* **1995**, *20*, 970−972.
(34) *Explicit Time-Domain Solutions of Maxwell's Equations Using Non-Orthogonal and Unstructured Grids*; Taflove, A., Ed.; Artech House: Boston, 1995.
(35) Goodman, J. J.; Draine, B. T.; Flatau, P. J. *Opt. Lett.* **1991**, *16*, 1198−1200.
(36) Draine, B. T.; Flatau, P. J. *User Guide for the Discrete Dipole Approximation Code DDSCAT6.0*, 2003.
(37) Jana, N. R.; Gearheart, L.; Murphy, C. J. *J. Phys. Chem. B* **2001**, *105*, 4065−4067.
(38) Johnson, C. J.; Dujardin, E.; Davis, S. A.; Murphy, C. J.; Mann, S. *J. Mater. Chem.* **2002**, *12*, 1765−1770.
(39) Nikoobakht, B.; El-Sayed, M. A. *Chem. Mater.* **2003**, *15*, 1957−1962.
(40) Wang, Z. L.; Mohamed, M. B.; Link, S.; El-Sayed, M. A. *Surf. Sci.* **1999**, *440*, L809−L814.
(41) Miller, M. M.; Lazarides, A. A. *SPIE, San Diego, CA, 2005*; Stockman, M. I., Ed.; San Diego, CA, 2005; Vol. 5927; pp 71−83.
(42) Averitt, R. D.; Westcott, S. L.; Halas, N. J. *J. Opt. Soc. Am. B* **1999**, *16*, 1824−1832.
(43) Oldenburg, S. J.; Averitt, R. D.; Westcott, S. L.; Halas, N. J. *Chem. Phys. Lett.* **1998**, *288*, 243−247.
(44) Prodan, E.; Nordlander, P.; Halas, N. J. *Nano Lett.* **2003**, *3*, 1411−1415.
(45) Neeves, A. E.; Birnboim, M. H. *J. Opt. Soc. Am. B* **1989**, *6*, 787−796.
(46) Prodan, E.; Nordlander, P.; Halas, N. J. *Chem. Phys. Lett.* **2003**, *368*, 94−101.
(47) Prodan, E.; Lee, A.; Nordlander, P. *Chem. Phys. Lett.* **2002**, *360*, 325−332.
(48) Miller, M.; Lazarides, A. Controlling the Sensing Volume of Metal Nanosphere Molecular Sensors. In *Material Research Society Symposium Proceedings*; San Francisco, CA, 2004; Vol. 820.